Accepted Manuscript

Nano-cement composite with graphene oxide produced from epigenetic graphite deposit

Tanvir S. Qureshi, Daman K. Panesar, Boopathi Sidhureddy, Aicheng Chen, Peter C. Wood

PII: S1359-8368(18)32675-1

DOI: 10.1016/j.compositesb.2018.09.095

Reference: JCOMB 6065

To appear in: *Composites Part B*

Received Date: 19 August 2018

Revised Date: 21 September 2018

Accepted Date: 28 September 2018

Please cite this article as: Qureshi TS, Panesar DK, Sidhureddy B, Chen A, Wood PC, Nano-cement composite with graphene oxide produced from epigenetic graphite deposit, *Composites Part B* (2018), doi: https://doi.org/10.1016/j.compositesb.2018.09.095.

Nano-cement composite with graphene oxide produced from epigenetic graphite deposit

Tanvir S Qureshi[a], Daman K Panesar[a*], Boopathi Sidhureddy[b], Aicheng Chen[b], and Peter C. Wood[c]

[a] Department of Civil and Mineral Engineering, University of Toronto, Toronto, Ontario M5S 1A4, Canada

[b] Electrochemical Technology Centre, Department of Chemistry, University of Guelph, Guelph, Ontario N1G 2W1, Canada

[c] Zenyatta Ventures Ltd., 1224 Amber Drive, Thunder Bay, Ontario P7B 6M5, Canada

*Corresponding author: d.panesar@utoronto.ca; Tel.: +1-416-946-5712

Abstract

This study presents the development of a nano-cement composite with graphene oxide (GO) carbon-based nanomaterials synthesized from a high-purity epigenetic graphite deposit. Diamond drill sampled graphite mineralization was upgraded through beneficiation and purification to recover a high-purity graphite product (99.9% graphitic carbon "Cg"). An alternate and improved chemical oxidation process based on the Modified Hummers method was adopted for the synthesis of GO from high-purity graphite. Microstructural analysis were performed to characterize GO. The GO consists of –OH, -C=O, -COOH, and C-O-C functional groups with a layer thickness of 1.2 nm, 2 to 3 layers of graphene, an interlayer distance of 0.89 nm and a Raman (I_D/I_G) ratio of 0.79. The effect of 0.02, 0.04, and 0.06 wt.% GO of cement on the composite workability, hydration, microstructure, mechanical and transport properties was determined. Increasing the concentration of GO in the composite decreased the workability due to the hydrophilic nature of the 2D planar surface. The rate of hydration accelerated and the cumulative hydration heat increased with the increasing proportions of GO in the composite. GO dosages about 0.02 and 0.04 wt.% of cement in the composites resulted the maximum enhancement of compressive and flexural strength by 83 and 26%, respectively, compared to the control mix (0 wt.% GO). The microstructural investigation shows that GO enhanced the hydration of calcium hydroxide (CH) and calcium silicate hydrate (C-S-H) during the nucleation and growth stages, filled pores, bridged micro-cracks and created interlocking between the cement hydration products. Collectively, these effects ultimately improved the mechanical properties of the composites. Also, in this process, the 0.02 and 0.04 wt.% GO cement composite increased the electrical resistivity by 11.5%, and decreased the sorptivity by 29%, respectively, both of which improved the overall performance of the composite.

Keywords: high-purity graphite, carbon-based nanomaterials, graphene oxide (GO), functional groups, micro-crack bridging.

1. Introduction

Reinforcement in cement-based materials can improve the physical properties and toughens the matrix. Graphene materials produced from graphite, namely, graphene oxide (GO) is a carbon-based nanomaterial, which is highly dispersible in water and poses useful physicochemical and mechanical properties. This nanomaterial has opened a new prospect to modify and reinforce cement-based composite materials at the micro-molecular level.

Graphite is a naturally occurring crystalline form of carbon typically found in platelet-shaped and needle forms within mineral deposits. Graphite deposits are generally formed by three different processes [1]:

i. Contact metamorphism of coal deposits: Graphite from this type of deposit is characterized by incomplete structural ordering and crystallization, resulting in low value "amorphous" graphite.

ii. Syngenetic flake graphite deposits: The formation of these deposits involves the alteration of carbonaceous organic matter to graphite during regional metamorphism. Regional metamorphism occurs when the mineralogy and texture of rocks are changed over a wide area due to deep burial (pressure) and heating associated with the large-scale forces of plate tectonics.

iii. Epigenetic graphite deposits: The formation of these deposits is associated with migrating supercritical carbon-bearing (C-O-H) fluids or fluid-rich magmas. The formation of the carbon-bearing fluids is most often a consequence of high temperature (granulite facies) metamorphism, but magmatic degassing can also produce graphite. Fluid precipitated graphite is well-ordered and can be a source of highly valued crystalline lump or vein-type (hydrothermal) graphite. This is the rarest type of graphite mineral deposit.

Graphene is a carbon-based nanomaterial where σ-bonds hexagonally connect each carbon atom to its three neighbors with sp^2 hybridisation formed in a one atomic thick 2D monolayer carbon sheet. There are different forms of graphene materials, and the difference lies in the number of layers [2] and functional groups on its edges and surfaces [3]. In graphite, graphene staking could be present in rhombohedral (ABCABCABC…) and hexagonal (ABABAB…) staking forms. Epigenetic graphite deposits exhibit highly crystalline and possess rhombohedral staking, which would be beneficial for the fabrication of desirable graphene derivatives. Graphene oxide (GO) is a graphene derivative which has various oxygen-containing functional groups, mainly hydroxyls (-OH) and epoxides (C-O-C) on their basal planes and carboxyls (-COOH) on the edges [4,5]. GO was also reported to contain carbonyl groups (-C=O) [6]. These functional groups make GO amorphous, yet highly dispersible in water. The oxygen-containing functional groups of GO has different binding energy with other atoms and molecules [4,5,7]. For example, the interaction affinity of GO functional groups increased in order of GO(-OH) < GO(-COOH) [7]. GO is stable in aqueous solutions. However, the size diameter was reported to increase from 240 nm to 6700 nm for the pH to decrease from 3.0 to 1.0 in an aqueous

solution [4]. The increase in GO diameter in an aqueous solution of a pH below 3.0 is due to the protonation of carboxyl groups at the edges of the GO plane [4]. The functional groups of GO can be reduced to produce reduced graphene oxide (rGO), which has good adsorption of aromatic compounds [8,9]. GO is synthesized from graphite, and the most convenient method to produce bulk quantities of GO is by the chemical oxidation and exfoliation of graphite [3,10]. The unique physicochemical properties and water dispersibility of GO produced from epigenetic graphite type ore could be suitable for incorporation in the cement-based composite to uniformly modify the matrix at the micro-nano level.

Studies in the last five years suggest that GO can improve the mechanical properties of nano-cement composites and densifies the matrix [11–21]. GO influences the cement hydration and modifies the pore distribution in the matrix [11–15,20]. The varying plane areas of GO (1-200 μm^2) was reported to decrease large pores (>1 µm diameter), decrease capillary pores (0.1-1 µm diameter) and increase small pores (1-45 nm diameter) in the composite [11]. Pores smaller than 10 nm in diameter are primarily gel pores contained within the C-S-H gel. Mokhtar et al. [16] investigated GO with a layer thickness less than 100 nm and a size of 1-2 µm within the range of 0.01 to 0.05 wt.% of cement in the paste composite. They reported that 0.02 and 0.03 wt.% GO of cement in the composites improves tensile strength and compressive strength by 13 and 41%, respectively, compared to the plain cement mix (100% cement). A GO with a C/O ratio of 1.36-0.98 and specimens with 0.08 wt.% GO of cement in the composite results maximum increase of the compressive strength by 46.8%, compared to the plain cement paste [17]. However, in the same study [17], specimens with GO 0.04 wt.% of cement in the composite results maximum increase of the flexural strength by 14.2%, compared to the plain cement paste. Recently, the use of GO at concentrations of 0.04 and 1.0 wt.% of cement in the composite is also reported to increased compressive strength by 25% and 47%, and flexural strength by 20% and 44%, respectively, compared to plain cement paste [21]. Although limited studies have investigated the influence of GO on the transport properties of the GO cement composites, reports indicate an increase in early age (24 h) electrical resistivity [17], and a decrease in chloride permeability in 28 days samples [18].

Studies on the GO cement composites typically report on either GO or graphite for GO synthesis from commercial sources [11,12,14–21] with limited or no information on the purity and grade of graphite. The purity of graphite used for GO synthesis and modification of the synthesis process can influence the characteristics of the GO and the corresponding GO cement composite. For example, Mokhtar et al. [16] and Qiu et al. [19] studied a similar GO dosage (0.02 wt.% of cement) and water to cement ratio (0.30) of the cement-based composite and reported considerably different performance. Graphite used in each of the studies was from different commercial sources which may have impacted the characteristics of the synthesised GO and the corresponding composites [16,19].

The objectives of this study are two-fold:

(i) To develop GO nanomaterials from a high-purity graphite (99.9% Cg) collected from an epigenetic graphite deposit with the improved synthesis methods, and

(ii) To determine the impact of varying concentrations of GO on the plastic and hardened properties of the cement-based composite.

2. Materials and Method

2.1 Materials

General use (GU) cement supplied by CRH Mississauga (Ontario, Canada) was used in this study. The chemical composition of GU cement is shown in Table 1. High-purity graphite (99.9% Cg) was supplied by Zenyatta Ventures Ltd. after purification from their Albany graphite deposit which is located in northeastern Ontario (Canada) (Fig. 1). Zenyatta's Albany graphite deposit is a unique example of an epigenetic graphite deposit, in which a large volume of highly crystalline and fluid-deposited graphite exists within an igneous host. The deposit is interpreted as a vent pipe breccia (fragmented rock) that formed from CO_2-rich fluids that evolved due to the pressure-related degassing of the intrusive rocks of the host alkalic complex [22]. The Albany graphite deposit is hosted in two large conical (carrot-shaped) breccia pipes (Fig. 1b) and is the largest and only igneous-hosted, fluid-derived graphite deposit of its kind in the world. These are thought to be created from a focused explosive volcanic event which broke up the rocks within the pipes, to form breccias, which have a graphite-rich matrix. The unusual deposit genesis accounts for the graphite's favorable crystallinity and fine particle size. The average graphite grade of the in-situ, in the ground, deposit is approximately 4% Cg (graphitic carbon, i.e. total carbon in graphite form) due to the abundant silicate gangue minerals. According to Conley and Moore [22], the Albany graphite crystals and crystal aggregates are up to 300 μm long and 50 μm wide; however, the average size of individual crystals is typically <100 μm. The unclassified high purity concentrate has a D50 of 20 to 25 μm. The D50 is the diameter of the particle the sample mass has 50% smaller particles and 50% larger of the total sample.

Table 1. The chemical composition (%) of GU cement.

SiO_2	Al_2O_3	Fe_2O_3	CaO	MgO	SO_3	Total Alkali	Free Lime	Loss on ignition
19.3	5.50	2.70	61.20	2.60	4.00	0.92	0.60	2.50

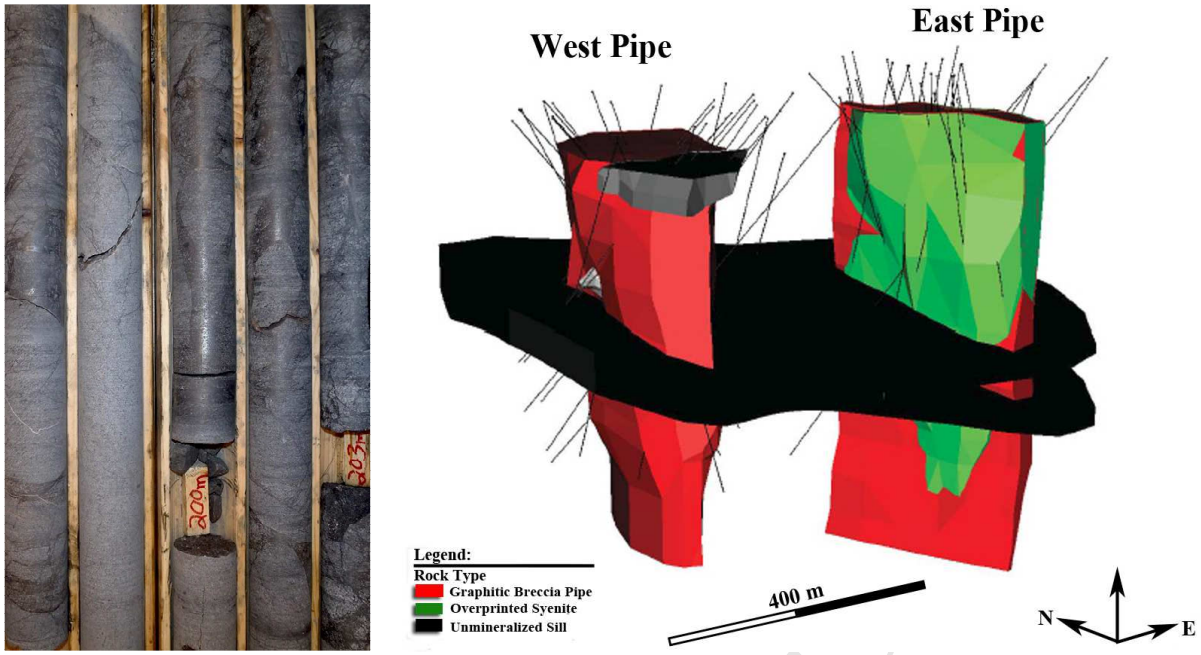

(a) (b)

Fig. 1. Igneous-hosted, fluid-derived epigenetic graphite mineralization in the Albany deposit, (a) typical drill core, and (b) graphitic breccia 3D view of wireframe model [23].

GO from graphite was synthesized using the following chemicals: sulfuric acid (98%, Sigma Aldrich), phosphoric acid (85%, Fisher), hydrochloric acid (35%, Sigma Aldrich), hydrogen peroxide (30%, Sigma Aldrich), ethanol (Green Field Inc.) and diethyl ether (BDH chemicals). Water was purified using Nanopure® diamond^{TM} UV water purification system, and used for aqueous solution preparation and washing.

Table 2 shows the mix proportions of the GO cement composites. To prepare the composite, GO was first dispersed in water following three steps: (i) GO powder was mixed with deionized water for 3 hr at 1000 rpm, ii) the mixture was sonicated for 2 hr, and iii) the GO solution was further stirred for 1 hr and sonicated for 1 hr prior to casting of the composite. The GO cement composite was mixed following ASTM C1738 [24] protocol.

Table 2. Mix composition of GO cement composites.

Mix	GO (wt.% of cement)	Cement (g)	GO (g)	Water content (mL)		
				Distilled water	Water with 5mg/mL GO	Total water
Control	0.00	3000	0.0	1350	0	1350
0.02% GO	0.02	3000	0.6	1200	150	1350
0.04% GO	0.04	3000	1.2	1050	300	1350
0.06% GO	0.06	3000	1.8	900	450	1350

2.2 Methods

2.2.1 Production of graphite from mineralization

Graphite was synthesis by the Grind, Float & Caustic Baking (NaOH) process as described by RPA Inc. [23]. In brief, the graphite mineralization 3 to 5% Cg collected by diamond drill was upgraded through beneficiation (crushing, grinding and flotation) to over 70% passing the 2 mm sieve, and a 1000 g split of the crushed material is pulverised to over 85% passing 75 microns sieve. Then through purification (caustic (NaOH) leaching and baking, mild sulphuric acid leach, and impurity precipitation), a high-purity graphite (99.9% Cg) was produced. This process is more environmentally friendly compared to other typical aggressive acid and thermal treatment based processes.

2.2.2 Synthesis of graphene oxide

The Modified Hummers method was adopted for the synthesis of GO with some alterations [25,26] . Briefly, 2.0 g of Albany high-purity graphite powder was added into a mixture of 180 mL H_2SO_4 and 20 mL H_3PO_4, and this reaction mixture was vigorously stirred at 50 °C for 2 h. Then 9.0 g of $KMnO_4$ was added, and the mixture was stirred for 15 h at 50 °C. The mixture was subsequently transferred into a 200 mL ice containing reaction container with 10 mL H_2O_2. The solid GO mixture was then isolated by centrifugation. Afterwards, the solid GO mixture was thoroughly rinsed with pure water, HCl (30 wt.%), and ethanol, and then soaked in diethyl ether. Finally, the resulting GO was dried for 16 hr at 50 °C. The layer numbers of GO was controlled to single or few layers by the duration of the oxidation process and the ratio of graphite and oxidants ($KMnO_4$ and H_2SO_4) used in the synthesis.

2.2.3 Characterisation of graphite and graphene oxide

A field-emission scanning electron microscope (SEM) (Hitachi SU-70) equipped with Energy Dispersive X-ray analysis (EDX) was used to characterise the morphology and surface composition of the graphite and the synthesized GO. A Pananalytical Xpert Pro Diffractometer with Ni-filtered monochromatic Cu Kr (1.5406 Å, 2.2 KW Max) was employed for the X-ray diffraction (XRD) analysis. To quantify the defect density of the synthesized samples, micro-Raman analysis was performed using a 514-nm laser excitation. An Agilent atomic force microscope (AFM) was employed to analyse and measure the thickness of the GO sheets.

2.2.4 Testing procedure for the cement paste composite

The workability of the composites was assessed through a mini-slump test with a mini cone having top diameter 19 mm, bottom diameter 38 mm, and a height of 57 mm. The static and dynamic flow diameters were measured according to [27] and ASTM C1437-07 [28], respectively. However, during the dynamic flow test, the table was raised and dropped 15 times instead of 25 times (where the latter

is according to the standard) to avoid the paste spread over the diameter of the table (25 cm.). The purpose of mini-slump testing was to study the influence of GO on the workability of the paste composite.

The early age hydration kinetics of the composite paste was measured using a thermometric TAM air calorimeter. The calorimeter began to record heat release data after the cement was in contact with water or GO solution for 5±1 min. The heat released from the hydration was monitored every 60 s for 72 h and the measured data was normalized by the sample mass.

To examine the influence of GO on the mechanical properties of the composite, compressive strength and flexural strength were measured on 28 days samples. The compressive strength test was performed on 50 mm cubes according to ASTM C109 [29] using a Forney 440 kN compression testing machine at a loading rate of 2.4 kN/s. The flexural strength test was performed on prisms (25x25x100 mm) by the three-point bending tests on an Autograph AG-I, Shimadzu 50 kN testing machine following ASTM C348 [30].

The microstructure of the composite samples was analysed by thermogravimetric analysis (TGA), XRD, and SEM. TGA was conducted on samples at day 1, 7 and 28 using a Netzsch thermische analyse STA 409 cell. The test was commenced at room temperature (25 ± 1 ^{o}C) and increased to 1000 ^{o}C over 102 minutes. The XRD patterns of the samples were measured using a Philips PW 3710 x-ray diffractometer at day 1, 7 and 28. Scanning ranged between 5-70^{o} of 2θ at a rate of 1.25 s/step and a scanning resolution of 0.02 ^{o}/step. The SEM imaging was performed on fragments of samples collected from the central parts of prisms that had been cured for 28 days, using a JEOL JSM-6610LV SEM machine. To make the samples conductive, a thin layer of gold was deposited onto the samples by a sputter deposition coating process.

Electrical resistivity and water sorptivity tests were performed to analyse the transport properties of the composites to provide an indication of durability performance. The electrical resistivity was measured on 50 mm cubes according to the uniaxial two-electrode method described in [31,32] using a GIATEC Scientific RCON concrete resistivity meter from 1 day to 28 days. A liquid capillary sorptivity test was performed on 50 mm cubes following the detailed procedure described in [33]. The sorptivity coefficient was measured using following Equation 1:

$$M_w = S\sqrt{t} \text{ ----------(1)}$$

where M_w is the water suction quantity per unit area and S is the sorptivity coefficient of the cube samples, and the square root of time t. Cube samples for the sorptivity test were collected after 28 days of curing in water, then the surface water of the samples was wiped with towels and the samples were placed in a vacuum dry desiccator with silica gel, at a temperature of 23±1 ^{o}C for 4 days. The

mass changes were within 0.1% in a 24 h period (between third and fourth days) drying prior the sorptivity test.

3. Results and discussion

3.1 Characterisation of graphite and graphene oxide

Fig. 2a shows the morphology of graphite particles with a layered structure. The epigenetic graphite was treated in the presence of strong oxidizing agents ($KMnO_4$ and H_2SO_4). These oxidizing agents could penetrate into the layered graphite structure and create oxygen-containing functional groups on both the edges and basal planes, resulting in the formation of GO. The GO planes were wrinkled after chemical oxidation in the harsh acid environment. A typical wrinkled GO layered structure is shown in the Fig. 2b. A high magnification SEM image of GO (Fig. 2c) provides a closer view of the wrinkled surface structure. The EDX analysis was performed to measure the chemical composition of the GO and was calculated to be 65.35 at% and 34.05 at% for carbon and oxygen, respectively. The synthesized GO contains graphene layers with –OH, -C=O, -COOH, and epoxy functional groups, which have been similarly reported by other authors [34,35]. Further, to confirm the exfoliated GO layers, AFM analysis was performed. The AFM image is shown in Fig. 3. The layer thickness was measured to be 1.2 nm, which indicates that the GO consists of 2 to 3 layers of graphene.

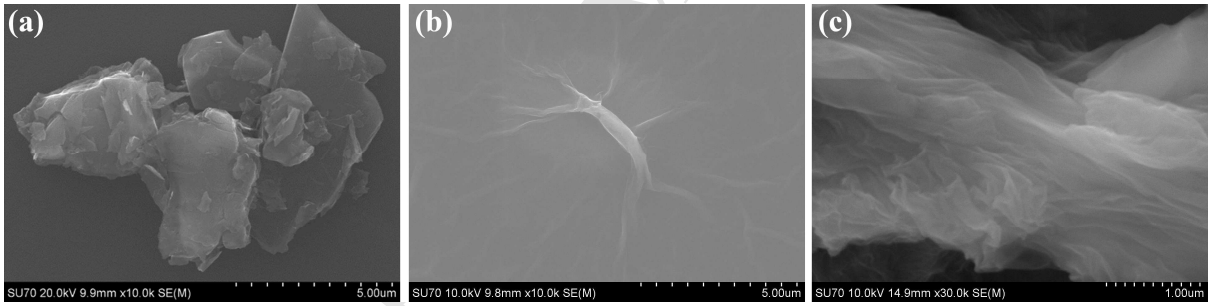

Fig. 2. FE-SEM images of, (a) graphite, (b) GO at X10,000 magnification, and (c) GO at X30,000 magnification.

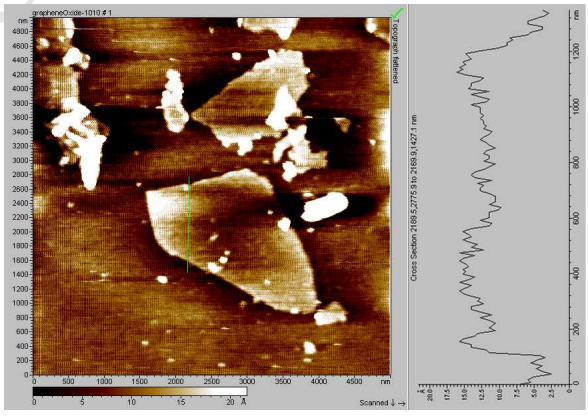

Fig. 3. AFM image of the synthesized graphene oxide.

Fig. 4a shows the XRD patterns of graphite and GO. The characteristic 2θ of graphitic carbon peak (002) occurs at 26.27°. The graphitic carbon XRD peak is not present in GO after it underwent chemical oxidation of graphite for GO synthesis. The major XRD peak for GO is appeared at 9.84° due to the effective oxidation of graphite. This chemical oxidation subsequently increases the interlayer distance of the graphene layers. The corresponding interlayer distance of graphite was 0.34 nm and for GO, increased to 0.90 nm after chemical oxidation. This is due to the introduction of the oxygen-containing functional groups in GO. Further, the crystallite length along C_{axis} (*Lc*) and the number of layers (*N*) were calculated from the XRD pattern using Equation 2 and 3, respectively [36].

$$Lc = \frac{0.90 \times \lambda}{(\beta \times \cos\theta)} \text{ ---------- (2)}$$

$$number\ of\ layers(N) = \frac{Lc(nm)}{d(nm)} \text{ ---------- (3)}$$

where, λ= wavelength of X-ray used for analysis 1.54056 Å; β= Full-width half maxima of the peak of <0 0 2> plane, and *d* is the interlayer spacing. The average number of layers was calculated to be 80 and 11 for graphite and GO, respectively.

The GO powder sample for XRD analysis was partially exfoliated and graphene layers may have been aggregated which indicated a high number of layers, i. e. 11. However, the GO was further exfoliated by dispersing it in solvents using ultrasonication and mechanical mixing prior to AFM analysis. The AFM measured layer thickness indicated 2 to 3 layers of graphene (Fig. 3). Since GO dispersion in water was used for composite preparation, the number of layers indicated by AFM is considered to be more accurate than those based on XRD calculations.

The Raman spectra of graphite and GO are presented in Fig. 4b. The variation in the intensity of the peaks for both graphite and GO were at 1350 and 1570 cm^{-1}, which corresponds to the D and G band, respectively. The ratio of the D band to the G band indicates the defect density (I_D/I_G) of the sample. After the chemical oxidation of graphite, the defect density of the resulting GO increased from 0.10 to 0.79. Further, the crystallite length (La) was calculated from the I_D/I_G ratio and wavelength (λ_l) using Equation 4 [37]. The crystallite size was measured to be 21.14 nm and 175.49 nm for the GO and graphite, respectively.

$$La = (2.4 \times 10^{-10}) \times \lambda_l^4 \times \left(\frac{I_D}{I_G}\right)^{-1} \text{ ---------- (4)}$$

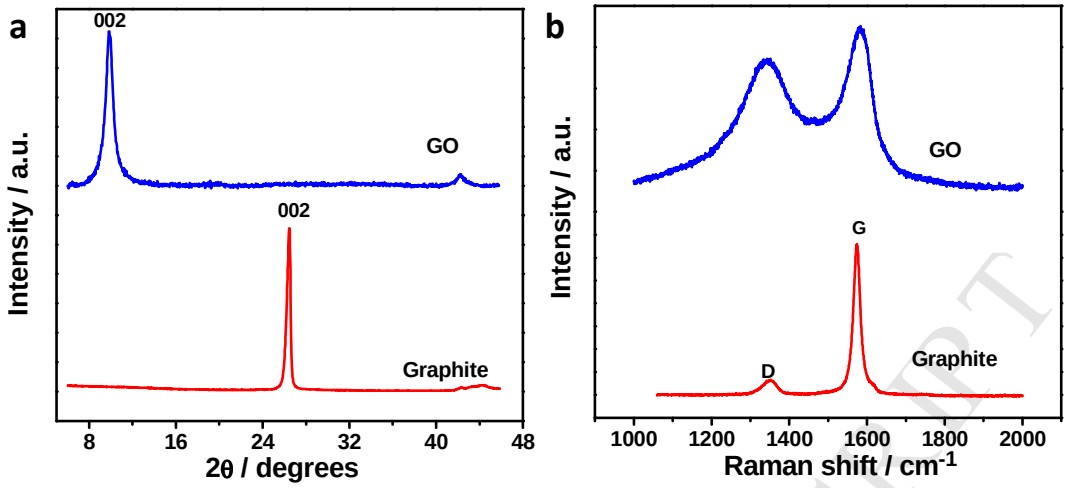

Fig. 4. (a) XRD pattern of Graphite and GO. (b) Raman spectra of Graphite and GO.

Key physical and microstructural parameters of graphite and GO are presented in Table 3. Clearly, the oxidation process results in a decrease in the graphite crystallite size and the number of layers, while the addition of the functional groups results in an increased interlayer *d* spacing, I_D/I_G ratio and oxygen atomic weight percentage. The improved synthesis of GO from graphite results in stable forms of GO with 2 to 3 graphene layers, uniform physical properties and optimum oxygen-containing functional groups. This form of GO is also highly dispersible in water and is favourable for efficiently mixing with cement to produce nano-cement composite.

Table 3. Physical properties and elemental composition of purified graphite and GO.

	Physical properties					Elemental composition (wt.%)	
	Crystallite size (nm)	*d* spacing (nm)	Layer thickness (nm)	Raman (I_D/I_G)	Number of layers	C	O
Purified graphite	175.49	0.34	Not measured	0.10	80	99.9	--
GO	21.14	0. 90	1.2	0.79	2 to 3	65.35	34.05

3.2 Workability of composites

The static and dynamic flow diameters from the mini-slump test are presented in Table 4. The results show that the workability decreases with the increasing concentrations of GO added to the cement composite paste. Both the static and dynamic flow diameters for the 0.02% GO cement composite decreased by 7.0 and 6.5%, respectively, compared to the control mix. The static flow diameter decreased by 21% in the 0.04% GO and 0.06% GO cement composite compared to the control mix. However, there was little change in the dynamic flow diameter in the 0.02% GO, 0.04% GO and 0.06% GO cement composite, compared to the control mix (8% decrease in 0.06% GO cement composite). The impact of GO on the workability is likely due to the hydrophilic oxide functional

groups containing the relatively large surface area and high interlayer distance (0.90 nm) between the 2D planes, which requires extra water to wet their surfaces as well as to interact between the GO nano-planes and the cement particles.

Table 4. Workability of composites: static and dynamic flow mini-slump test.

Flow type	0% Control		0.02% GO		0.04% GO		0.06% GO	
	average	standard deviation	average	standard deviation	average	standard deviation	average	standard deviation
Static	66.33	1.53	61.67	1.58	52.33	0.58	52.50	0.50
Dynamic	126.0	1.00	117.80	2.60	117.30	1.60	115.60	1.60

3.3 Hydration kinetics

The rate and cumulative heat of hydration of the paste composites recorded by the calorimeter are shown in Fig. 5. The GO cement composite exhibited a higher rate of heat of hydration and cumulative heat compared to the control cement mix (0% GO). The cement hydration peak associated with C_3S (close to 7 h) and C_3A (close to 12.5 h) shows that the nucleation and growth stage was slightly increased and shifted to the left in the GO composites. The cumulative heat of hydration increased with the increasing concentrations of GO in the composite. This was due to an acceleration effect by the GO, which enhanced the rate of cement hydration in the nucleation and growth stages owing to its high surface area and active oxygen-containing functional groups. The effect of GO on cement hydration has been reported in the literature with similar observations [17,20]. The final setting times decreased for the 0.02% GO, 0.04% GO, and 0.06% GO cement composites by approximately 15, 21, and 24 min, respectively, compared to the control mix.

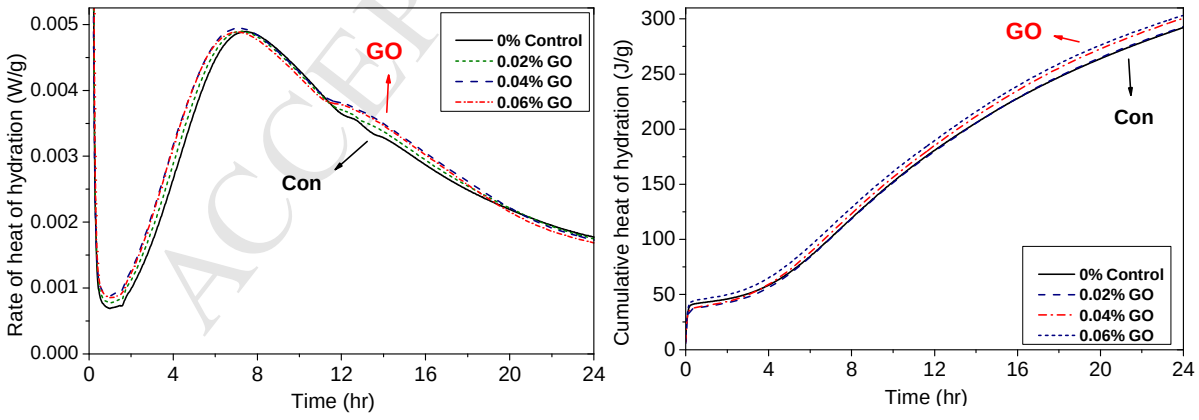

(a) (b)

Fig. 5. Effect of GO on the hydration of the composite over the first 24 h hydration: (a) rate of heat of hydration, (b) cumulative heat of hydration.

3.4 Mechanical properties

Compressive and flexural strength tests were conducted to investigate the impact of GO on the mechanical properties (Fig. 6). Compressive strength results are presented in Fig. 6a, and indicate that the GO improved the compressive strength of the composites at 28 days. Compared to the control mix, the compressive strength of the 0.02% GO, 0.04% GO and 0.06% GO cement composites increased by 6%, 26% and 12%, respectively. An increase in the GO dosage from 0.04 to 0.06% in the composite did not further improve the compressive strength, but instead shows a decreasing trend.

The improvement in flexural strength by GO in the composites was greater, compared to that of the compressive strength. The flexural strength of the 0.02% GO, 0.04% GO and 0.06% GO cement composites increased by 83%, 70% and 54%, respectively, compared to the control mix (Fig. 6b). However, the greatest flexural strength was achieved by the 0.02% GO cement composite, and in fact increasing the GO concentration resulted in a decrease in strength. Overall, the GO appears to reinforce the cement matrix at a nano-micro scale, which shows a net improvement in flexural strength with the addition of GO in the cement-based composite.

There are several reasons that the GO may have improved the compressive strength and flexural strength of the GO cement composite. Firstly, the large surface area with functional groups may have acted as nucleation sites, prompting hydration and the production of CH, C-S-H etc. Secondly, the uniform dispersion of the 2D nano planes provides reinforcement at nano-micro structural level. Finally, the GO might have also chemically cross-linked to the matrix through the influence of the oxide functional groups during the cement hydration process.

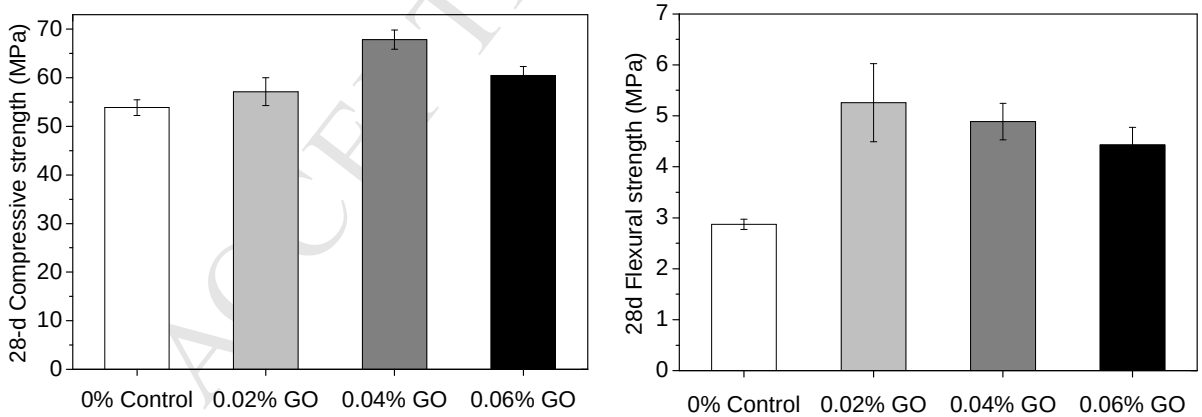

(a) (b)

Fig. 6. The mechanical strength at 28 days: (a) compressive strength, and (b) flexural strength.

It should be noted that no greater strength increases in the GO cement composite were observed beyond GO concentrations of 0.04 wt.% of cement. The greatest improvement of compressive and flexural strength was achieved by 0.04% GO and 0.02% GO cement composite, respectively. The

concentration of GO greater than 0.04 wt.% of cement may have provided extra nucleation sites and functional groups in the composite, but they have not contributed to the further enhancement of mechanical strength. Also the pH level of the GO solution decreases with increasing GO concentration. The control (0.0%), 0.02% GO, 0.04% GO, and 0.06% GO solutions had pH values of 6.94, 5.58, 3.14 and 3.09, respectively. Decreasing the pH levels with higher GO concentration acidifies the solution, which may have also had a negative impact on the cement hydration reactions.

3.5 Microstructure of composites

3.5.1 Thermogravimetric analysis

The TGA results of the composite samples at 1, 7 and 28 days are shown in Fig. 7. The weight loss percentage gradually decreases with the increasing temperature and the derivative thermogravimetric (DTG) curve has inflections, which correspond to the decomposition of the specific hydration phases. The TGA plots in Fig. 7a-c can be described corresponding to the following temperature range increments: (i) 30-105 ^{o}C: the evaporable water and part of the bound water escapes; (ii) 110-250 ^{o}C: C-S-H, C_2ASH_8, ettringite, AFm phases (alumina, ferric oxide, monosulfate phase), mono-carbonate; (iii) 400-500 ^{o}C: dihydroxylation of the CH; (iv) 650-800 ^{o}C: decarbonation of calcium carbonate. The degree of hydration of cement and GO cement composite is directly related to of the percentage of CH, which was calculated using the Equation 4:

$$\text{CH content (\%)} = (M_{CH}/M_{500}) \times (74/18) \times 100\ (\%) \text{ ----------(4)}$$

where, M_{CH} = the percentage weight loss of calcium hydroxide (CH: 400 to 500 ^{o}C), M_{500} = weight at 500 ^{o}C, and the fraction 74/18 is used to convert the CH bound water into the CH mass where 74 is the molar mass of CH and 18 is the molar mass of H_2O.

Fig. 7d presents the CH content (%) of the GO cement composites at 1, 7 and 28 days. Results show that the GO cement composites resulted in a greater mass loss of the CH content (%) compared to the control mix at all ages. At early age (1 day) the CH content (%) shows the trend of 0.06% GO> 0.02% GO > 0.04% GO > control. However, at 7 and 28 days, this trend alters to 0.06% GO> 0.04% GO > 0.02% GO > control, indicating that higher dosages of GO steadily influences the cement hydration process over time. While the calorimetric study indicated that GO accelerates the cement hydration process, the increase in the CH content (%) by GO in the composite further confirms it. The hydrophilic GO nanoplane with functional groups may absorb water molecules [38,39], which act as additional nucleation sites for cement hydration. Fig. 7a, b and c also show a minor increase in the carbonate phases of the DTG curve peaks, which may be due to the reaction of the –COOH functional group with adjoining CH phases leading to the formation of complex hydration products such as calcium carboaluminate hydrate [16]. The accelerated rate of cement hydration caused by the GO

confirms its influence on the cement hydration process. This can also yield the enhancement of the mechanical properties of the GO cement composites.

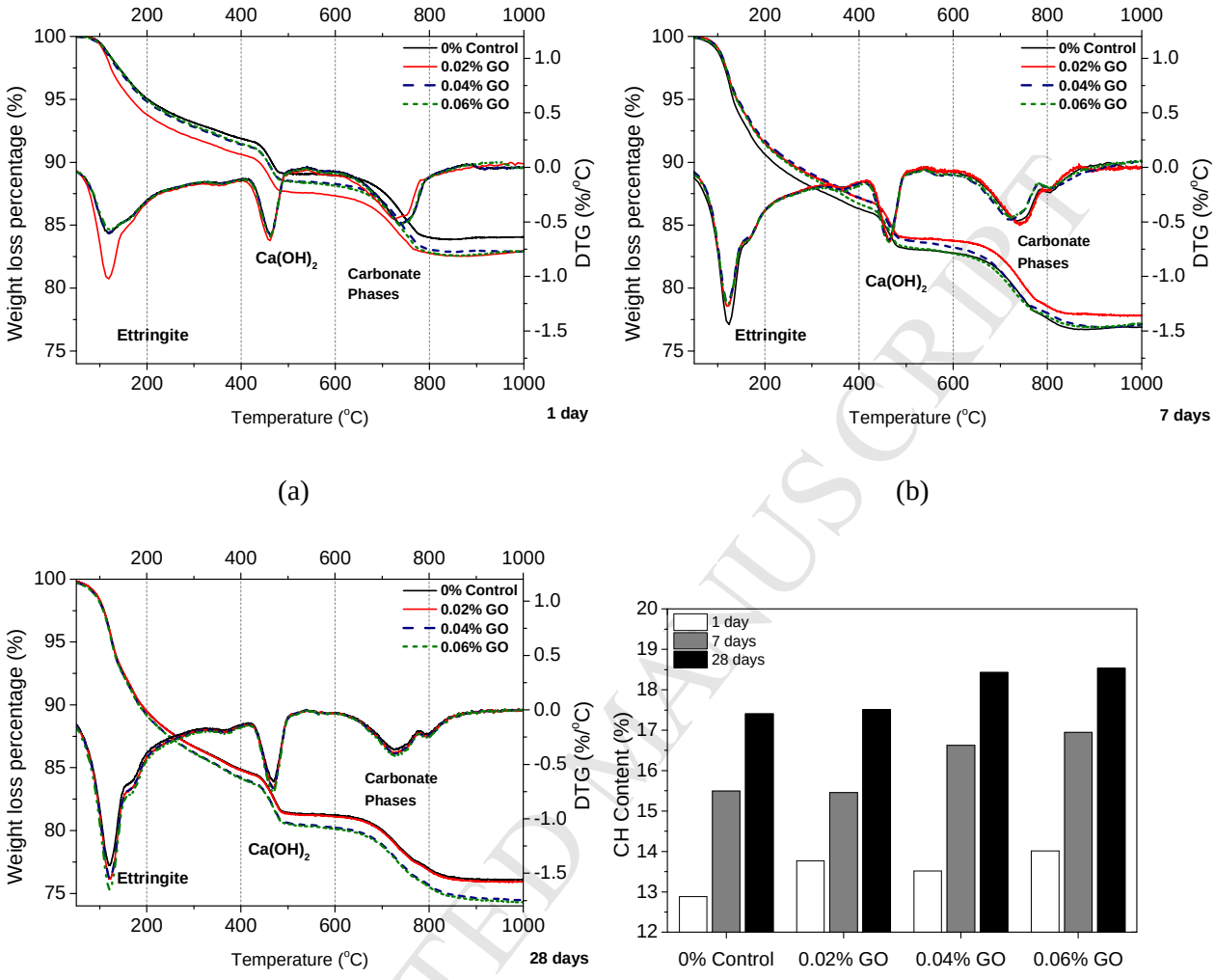

Fig. 7. TGA and DTG curves of the composite samples: (a) 1 day, (b) 7 days, (c) 28 days, (d) CH content (%) at day 1, day 7 and day 28.

3.5.1 X-ray Diffraction (XRD)

The XRD curves of 1, 7 and 28 days samples are presented in Fig. 8. Peak intensities indicate the typical cement hydration products such as ettringite, portlandite (CH), tricalcium silicate (C_3S), dicalcium silicate (C_2S) for all mixes at ages from day 1 to 28. No new material formation is indicated by XRD due to the impact of GO. However, the XRD patterns have good profile fitting (goodness of fit <2.5) by the Rietveld method to measure the crystalline and amorphous phases.

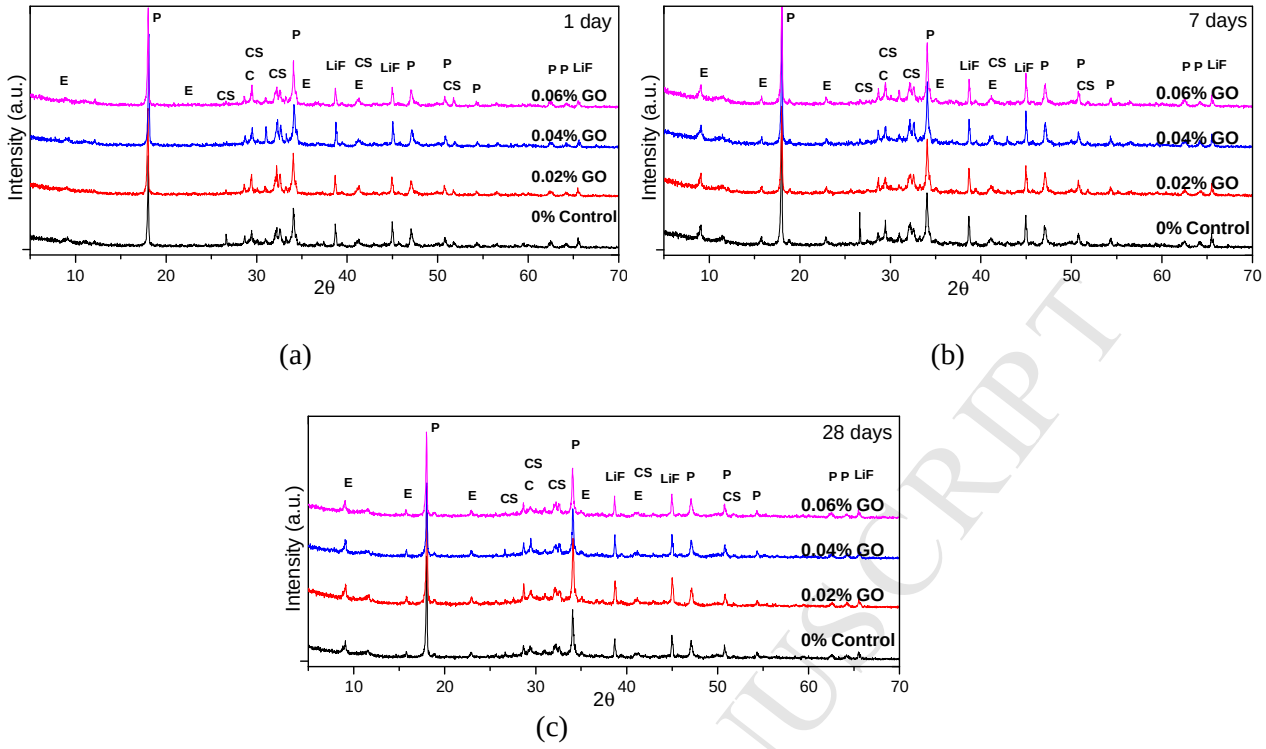

(a) (b)

(c)

Fig. 8. XRD curves of the composite samples (a) 1 day (24 hr hydration), (b) 7 days, and (c) 28 days. Graph notations: E= Ettringite, C= Calcite, CS= C_2S and C_3S, P= Portlandite (CH), LiF= Lithium fluoride), and (d) theoretical volume estimated by Rietveld method of 28 day hydrated samples.

The formation of three major cement hydration phases (CH, C-S-H, and ettringite) quantified by the Rietveld method is shown in Fig. 9. The percentage of CH shows an increasing trend with the increasing GO proportions and hydration age (Fig. 9a). The Rietveld CH (%) quantification results show good coherence with the TGA quantified values of the CH content (%), confirming the accuracy of the Rietveld method. The amount of C-S-H (%) in the hydrated GO cement composite is shown in Fig. 9b is quantified considering that the amorphous phase in hydrated GU cement is mostly C-S-H. The amount of C-S-H (%) also increases with the increase in GO proportion and hydration age. The increasing amount of both CH (%) and C-S-H (%) (with age and GO dosage) indicates that GO influences the cement hydration during the nucleation and growth stage acting as nucleation sites which triggers C_3S hydration. Ettringite is one of the primary products in cement hydration at an early age due to C_3A phase hydration. The percentage of ettringite increases from 1 day to 7 days then decreases at 28 days except for 0.06% GO cement composite, which shows an increasing trend from 7 days to 28 days (Fig. 9c). The ettringite formation was slightly higher in the 0.02% GO cement composite at 1 day compared to the control mix, and the amount of ettringite (%) was low at 7 and 28 days. The ettringite formation in the 0.04% GO cement composite at 1 day, and in the 0.06% GO cement composite at 1 and 7 days was lower compared to the control mix then slightly increases at 28 days. Therefore, higher proportions of GO shows a slight increasing trend in the amount of ettringite

(%) compared to the control mix with the age of cement hydration up to 28 days. These XRD results also correspond to the calorimetric hydration heat release studies.

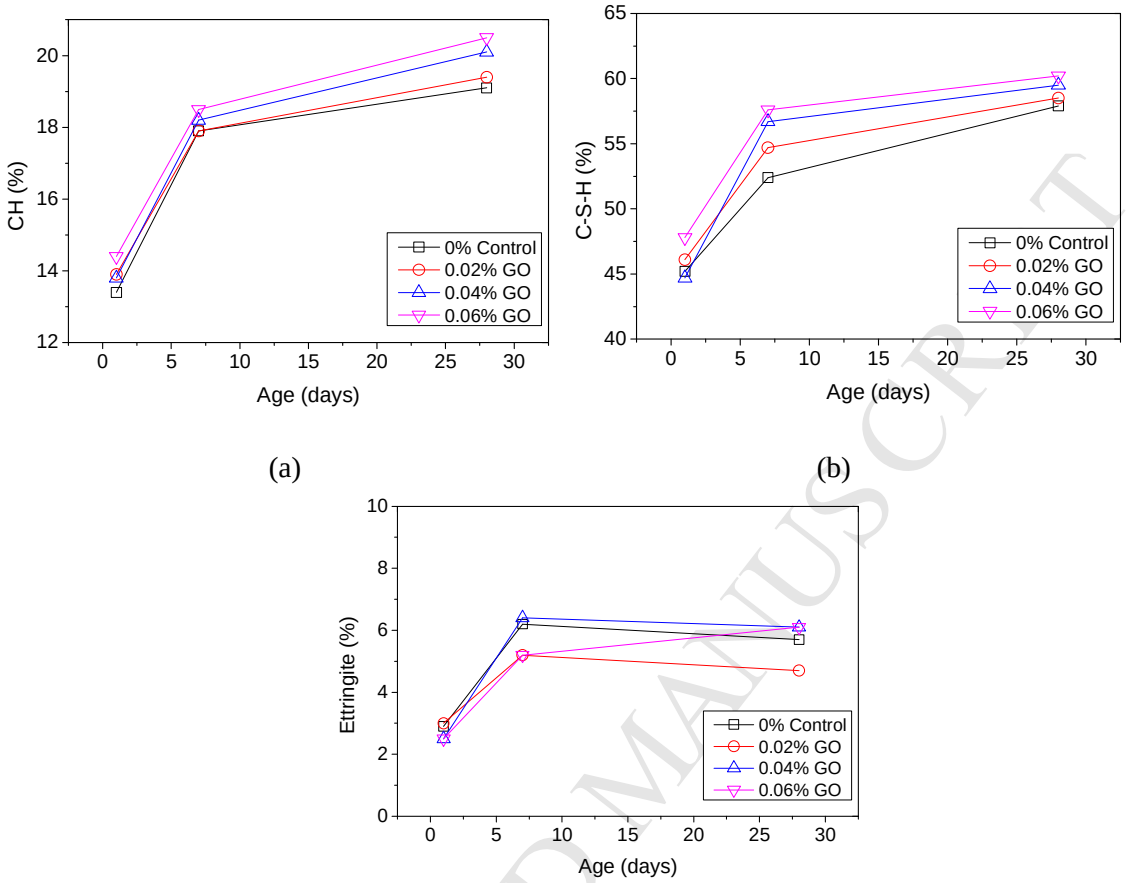

Fig. 9. Amount of major cement hydration products by Rietveld method, (a) CH, (b) C-S-H, and (c) ettringite.

3.5.3 Scanning electron microscopic (SEM) imaging

The SEM images of 28 day samples surface are presented in Fig. 10. The SEM image of the control mix revealed the typical non-uniform distribution of cement hydration products, micropores and microcracks (Fig. 10a). Fig. 10b and 10c, respectively show the crack bridging by GO as well as nano planes with cement hydration products in 5 µm diameter pore in the 0.02% GO cement composite. The GO acts as reinforcement at the nano-micro scale and bridges the cement hydration products through gel pores (Fig. 10 d and e). The functional groups on the GO plane may have reacted and encouraged the formation of hydration products, which developed chemical interlocking between hydration products and wrinkled planes of the GO. A high magnification SEM image also shows a typical micropore filling performance by the GO (Fig. 10f). The effective dispersion of GO in water

resulted in a uniform nano-cement composite distribution in the matrix which yeilds consistent improvement of the microstructure.

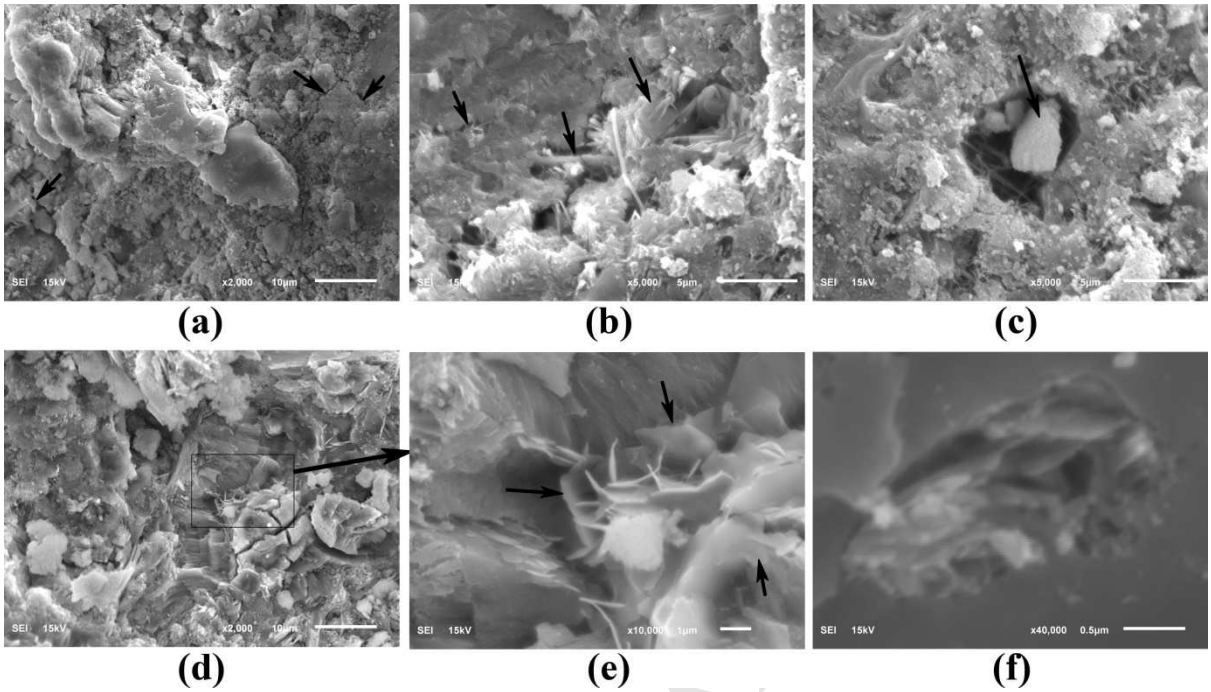

Fig. 10. SEM images of the composite surface 28 days: (a) micro cracks in the control mix, (b) crack bridging in 0.02% GO, (c) GO layer with hydration product on surface into 5 µm pore of 0.02% GO, (d) surface morphology of 0.04% GO, (e) 0.04% GO: hydration product bridging by GO at nano-micro scale, and (f) 1 µm pore filling by GO high magnification image (X40,000) on 0.06% GO.

The formation of hybrid materials and the chemical reactions between the carboxylic acid of GO and the C-S-H or portlandite are also similarly reported in other studies [11,20,21,39,40]. All of the effects of GO in the hydrated cement composite matrix such as enhancement in cement hydration, pore filling, micro-crack bridging and creating interlocking between cement hydration products ultimately improved the mechanical properties of composites. The influence of GO in cement hydration was also confirmed by the calorimetric study, TGA and XRD results.

3.5 Transport properties

Electrical resistivity and one-dimensional water sorptivity tests were performed to investigate the influence of GO on the transport properties of the composites (Fig. 11). Both the electrical resistivity and water sorption of the composites can indicate durability performance. For example, the higher the electrical resistivity and lower sorptivity coefficient, the denser the matrix microstructure, which in most cases has a positive impact on the durability performance of the composite [31,32]. The electrical resistivity gradually increases with hydration time for all of the mixes (Fig. 11a). The resistivity was found to be the highest in the 0.02% GO cement composite and it then decreases with

increasing GO content in the composites. Up to the first 5 days after casting, the resistivity improvement in the GO cement composites compared to the control mix was not noticeable. However, the difference in resistivity continued to increase as cement hydration proceeds. This is also in agreement with hydration and microstructural results that indicated the densification of composites by GO. The sorptivity coefficient of the hardened paste composites at 28 days was calculated according to Equation 1 and is shown in Fig. 11b. The sorptivity coefficient was reduced by 29% in the 0.04% GO cement composite compared to the control mix. Where the 0.02% GO and 0.06% GO cement composites show a reduction of 25% and 27% sorptivity coefficient, respectively, compared to the control mix. Homogeneous C-S-H gel material with the crystalline hydrated compound formation and strong covalent bonding in the cement matrix pores by GO may have resulted in this improved sorptivity performance. The sorptivity results also resemble the electrical resistivity of the composites. Therefore, the formation of a higher quantity of hydration products such as C-S-H gel and pore filling SEM images of the GO cement composites are in agreement with the transport property results.

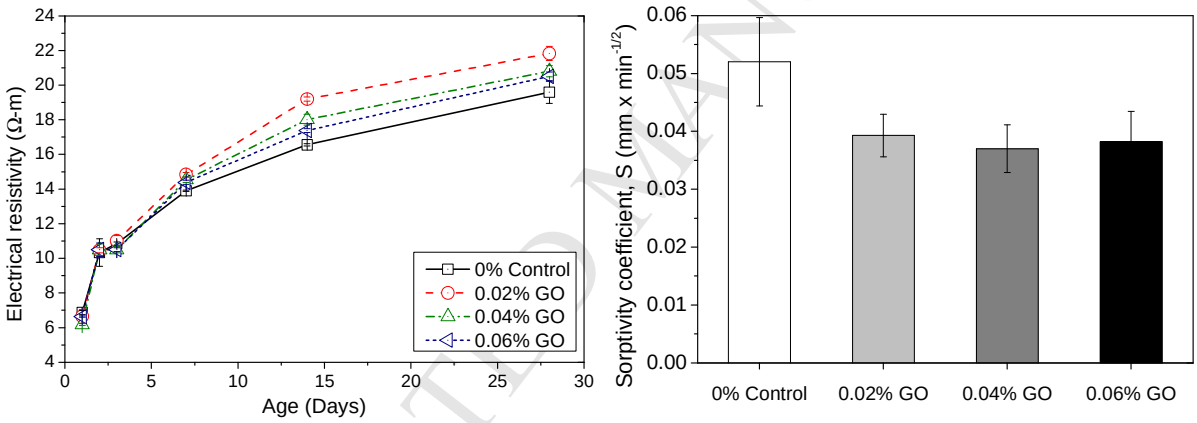

(a) (b)

Fig. 11. Transport properties: (a) electrical resistivity (day 1-28) and (b) water sorptivity coefficient (at 28 days).

4. Conclusions

This paper presents the synthesis approach of GO nanomaterials from high-purity graphite mineral and its influence on the properties of the GO cement composites. The influence of GO in the GO cement composites was investigated to evaluate its workability, hydration, microstructure, mechanical and transport properties. Key conclusions are summarised as follows:

- High–purity Albany graphite (99.9% Cg) was used as a precursor material to synthesize GO using an improved chemical oxidation process based on the Modified Hummers Method. The synthesized GO with the oxygen-containing functional groups have an interlayer distance of 0.90

nm, crystal size of 21.14 nm, with 2 to 3 layers of 1.2 nm thickness, and carbon and oxygen wt.% of 65.35 and 34.05, respectively.

- With the dosage of 0.06 wt.% GO of cement in the composite, both the static and dynamic flow diameters decreased up to 21% and 8%, respectively, compared to the control mix. The water demanding hydrophilic planes of GO captures extra water, which decreases the workability of the GO cement composites.
- The GO cement composite exhibited a higher rate of heat of hydration and cumulative heat than the control mix. This was due to enhanced nucleation through GOs large surface area and active oxygen-containing functional groups. Compared to the control mix, the final setting time decreased by 15, 20 and 25 min in the 0.02% GO, 0.04% GO and 0.06% GO cement composite, respectively.
- Greatest enhancement of the compressive strength was observed in the 0.04% GO cement composite paste, which was 26% greater than the control mix. Greatest enhancement of the flexural strength was observed in the 0.02% GO cement composite, which was greater than the control mix by 83%.
- The microstructural investigation shows that GO planes with oxygen-containing functional groups provided nucleation sites and reacted with the cement hydration products. This occurrence was observed to fill micropores and reinforces the composite matrix at a nano-micro scale, which enhances the mechanical properties of the composite.
- The incorporation of GO has improved both the electrical resistivity and water sorption properties of the GO cement composites. Compared to the control mix, the 0.02% GO cement composite exhibited an 11.5% increase in electrical resistivity. The sorptivity coefficient was reduced by 29% in the 0.04% GO cement composite compared to the control mix and was the greatest observed reduction in all GO mixes.
- Overall this research opens prospects to modify the cement-based composite system at nano-microscale to enhance its mechanical and transport properties. A stable and uniform graphene-based nanomaterial, (i.e. GO) was synthesised from a high-purity graphite (99.9% Cg), and used to produce the GO cement composite with improved properties. In the future, GO cement composites should be compared with the other forms of the graphene-based materials nano-cement composites. Also the study should be extended to investigate long-term properties and more complex cement based systems, such as mortar and concrete.

Acknowledgement

The authors are grateful for support from an NSERC Engage grant in collaboration with Zenyatta Ventures Ltd.

Reference

[1] Harben PW, Kuzvart M. A Global Geology London. London: Industrial Minerals Information Ltd.; 1996.

[2] Han B, Zheng Q, Sun S, Dong S, Zhang L, Yu X, et al. Enhancing mechanisms of multi-layer graphenes to cementitious composites. Compos Part A Appl Sci Manuf 2017;101:143–50. doi:10.1016/j.compositesa.2017.06.016.

[3] Gholampour A, Valizadeh Kiamahalleh M, Tran DNH, Ozbakkaloglu T, Losic D. From Graphene Oxide to Reduced Graphene Oxide: Impact on the Physiochemical and Mechanical Properties of Graphene–Cement Composites. ACS Appl Mater Interfaces 2017:acsami.7b16736. doi:10.1021/acsami.7b16736.

[4] Yu S, Wang X, Ai Y, Liang Y, Ji Y, Li J, et al. Spectroscopic and theoretical studies on the counterion effect of Cu(ii) ion and graphene oxide interaction with titanium dioxide. Environ Sci Nano 2016;3:1361–8. doi:10.1039/C6EN00297H.

[5] Wang X, Fan Q, Yu S, Chen Z, Ai Y, Sun Y, et al. High sorption of U(VI) on graphene oxides studied by batch experimental and theoretical calculations. Chem Eng J 2016;287:448–55. doi:10.1016/j.cej.2015.11.066.

[6] Lambert TN, Chavez CA, Hernandez-Sanchez B, Lu P, Bell NS, Ambrosini A, et al. Synthesis and Characterization of Titania−Graphene Nanocomposites. J Phys Chem C 2009;113:19812–23. doi:10.1021/jp905456f.

[7] Wang X, Liu Y, Pang H, Yu S, Ai Y, Ma X, et al. Effect of graphene oxide surface modification on the elimination of Co(II) from aqueous solutions. Chem Eng J 2018;344:380–90. doi:10.1016/j.cej.2018.03.107.

[8] Yu S, Wang X, Yao W, Wang J, Ji Y, Ai Y, et al. Macroscopic, Spectroscopic, and Theoretical Investigation for the Interaction of Phenol and Naphthol on Reduced Graphene Oxide. Environ Sci Technol 2017;51:3278–86. doi:10.1021/acs.est.6b06259.

[9] Yu S, Wang X, Ai Y, Tan X, Hayat T, Hu W, et al. Experimental and theoretical studies on competitive adsorption of aromatic compounds on reduced graphene oxides. J Mater Chem A 2016;4:5654–62. doi:10.1039/C6TA00890A.

[10] Alam SN, Sharma N, Kumar L. Synthesis of Graphene Oxide (GO) by Modified Hummers Method and Its Thermal Reduction to Obtain Reduced Graphene Oxide (rGO)*. Graphene 2017;06:1–18. doi:10.4236/graphene.2017.61001.

[11] Pan Z, He L, Qiu L, Korayem AH, Li G, Zhu JW, et al. Mechanical properties and microstructure of a graphene oxide–cement composite. Cem Concr Compos 2015;58:140–7. doi:10.1016/j.cemconcomp.2015.02.001.

[12] Horszczaruk E, Mijowska E, Kalenczuk RJ, Aleksandrzak M, Mijowska S. Nanocomposite of cement/graphene oxide - Impact on hydration kinetics and Young's modulus. Constr Build Mater 2015;78:234–42. doi:10.1016/j.conbuildmat.2014.12.009.

[13] Lv S, Ma Y, Qiu C, Sun T, Liu J, Zhou Q. Effect of graphene oxide nanosheets of microstructure and mechanical properties of cement composites. Constr Build Mater 2013;49:121–7. doi:10.1016/j.conbuildmat.2013.08.022.

[14] Gong K, Pan Z, Korayem AH, Qiu L, Li D, Collins F, et al. Reinforcing Effects of Graphene Oxide on Portland Cement Paste. J Mater Civ Eng 2015;27:A4014010. doi:10.1061/(ASCE)MT.1943-5533.0001125.

[15] Cui H, Yan X, Tang L, Xing F. Possible pitfall in sample preparation for SEM analysis - A discussion of the paper “Fabrication of polycarboxylate/graphene oxide nanosheet composites by copolymerization for reinforcing and toughening cement composites” by Lv et al. Cem Concr Compos 2017;77:81–5. doi:10.1016/j.cemconcomp.2016.12.007.

[16] Mokhtar MM, Abo-El-Enein SA, Hassaan MY, Morsy MS, Khalil MH. Mechanical performance, pore structure and micro-structural characteristics of graphene oxide nano platelets reinforced cement. Constr Build Mater 2017;138:333–9. doi:10.1016/j.conbuildmat.2017.02.021.

[17] Li W, Li X, Chen SJ, Liu YM, Duan WH, Shah SP. Effects of graphene oxide on early-age hydration and electrical resistivity of Portland cement paste. Constr Build Mater 2017;136:506–14. doi:10.1016/j.conbuildmat.2017.01.066.

[18] Mohammed A, Sanjayan JG, Duan WH, Nazari A. Incorporating graphene oxide in cement composites: A study of transport properties. Constr Build Mater 2015;84:341–7. doi:10.1016/j.conbuildmat.2015.01.083.

[19] Qiu C, Zhou Q, Lv S, Ma Y. Regulation of GO on cement hydration crystals and its toughening effect. Mag Concr Res 2013;65:1246–54. doi:10.1680/macr.13.00190.

[20] Zhao L, Guo X, Ge C, Li Q, Guo L, Shu X, et al. Mechanical behavior and toughening mechanism of polycarboxylate superplasticizer modified graphene oxide reinforced cement composites. Compos Part B Eng 2017;113:308–16. doi:10.1016/j.compositesb.2017.01.056.

[21] Chen ZS, Zhou X, Wang X, Guo P. Mechanical behavior of multilayer GO carbon-fiber cement composites. Constr Build Mater 2018;159:205–12. doi:10.1016/j.conbuildmat.2017.10.094.

[22] Conly AG, Moore LC. Geology, ore characteristics, and origin of the Albany graphite deposit. Br Columbia Geol Surv Pap 2015;3:173–85.

[23] RPA I. Technical Report on the Preliminary economic assessment of the Albany graphite project, northern Ontario, Canada. 2015.

[24] ASTM International. ASTM C1738, Standard Practice for High-Shear Mixing of Hydraulic Cement Pastes. 2011. doi:10.1520/C1738-11.

[25] Marcano DC, Kosynkin D V., Berlin JM, Sinitskii A, Sun Z, Slesarev A, et al. Improved Synthesis of Graphene Oxide. ACS Nano 2010;4:4806–14. doi:10.1021/nn1006368.

[26] Boopathi S, Narayanan TN, Senthil Kumar S. Improved heterogeneous electron transfer kinetics of fluorinated graphene derivatives. Nanoscale 2014;6:10140–6. doi:10.1039/c4nr02563f.

[27] Collins F, Lambert J, Duan WH. The influences of admixtures on the dispersion, workability, and strength of carbon nanotube-OPC paste mixtures. Cem Concr Compos 2012;34:201–7. doi:10.1016/j.cemconcomp.2011.09.013.

[28] ASTM Standard C1437-07. Standard Test Method for Flow of Hydraulic Cement Mortar. 2007. doi:10.1520/C1437-07.

[29] ASTM C109 / C109M-16a. Standard Test Method for Compressive Strength of Hydraulic Cement Mortars (Using 2-in. or [50-mm] Cube Specimens). 2016. doi:10.1520/C0109_C0109M-16A.

[30] ASTM C348-14. Standard Test Method for Flexural Strength of Hydraulic-Cement Mortars. 2014. doi:10.1520/C0348-14.

[31] Layssi H, Ghods P, Alizadeh AR, Salehi M. Electrical resistivity of concrete. Concr Int 2015;37:41–6.

[32] Sengul O. Use of electrical resistivity as an indicator for durability. Constr Build Mater 2014;73:434–41. doi:10.1016/j.conbuildmat.2014.09.077.

[33] Qureshi TS, Al-Tabbaa A. Self-healing of drying shrinkage cracks in cement-based materials incorporating reactive MgO. Smart Mater Struct 2016;25:084004. doi:10.1088/0964-1726/25/8/084004.

[34] Wu N, She X, Yang D, Wu X, Su F, Chen Y. Synthesis of network reduced graphene oxide in polystyrene matrix by a two-step reduction method for superior conductivity of the composite. J Mater Chem 2012;22:17254–61. doi:10.1039/c2jm33114d.

[35] Kadam MM, Lokare OR, Kireeti KVMK, Gaikar VG, Jha N. Impact of the degree of functionalization of graphene oxide on the electrochemical charge storage property and metal ion adsorption. RSC Adv 2014;4:62737–45. doi:10.1039/c4ra08862j.

[36] Roy Chowdhury D, Singh C, Paul A. Role of graphite precursor and sodium nitrate in graphite oxide synthesis. RSC Adv 2014;4:15138. doi:10.1039/c4ra01019a.

[37] Cançado LG, Takai K, Enoki T, Endo M, Kim YA, Mizusaki H, et al. General equation for the determination of the crystallite size La of nanographite by Raman spectroscopy. Appl Phys Lett 2006;88:163106. doi:10.1063/1.2196057.

[38] Babak F, Abolfazl H, Alimorad R, Parviz G. Preparation and mechanical properties of graphene oxide: cement nanocomposites. ScientificWorldJournal 2014;2014:276323. doi:10.1155/2014/276323.

[39] Yang H, Monasterio M, Cui H, Han N. Experimental study of the effects of graphene oxide on microstructure and properties of cement paste composite. Compos Part A Appl Sci Manuf 2017;102:263–72. doi:10.1016/j.compositesa.2017.07.022.

[40] Li X, Korayem AH, Li C, Liu Y, He H, Sanjayan JG, et al. Incorporation of graphene oxide and silica fume into cement paste: A study of dispersion and compressive strength. Constr Build Mater 2016;123:327–35. doi:10.1016/j.conbuildmat.2016.07.022.